

# DARWIN 1.5 : Large Language Models as Materials Science Adapted Learners

Tong Xie<sup>1,2\*†</sup>, Yuwei Wan<sup>2,3†</sup>, Yixuan Liu<sup>2</sup>, Yuchen Zeng<sup>4</sup>,  
Shaozhou Wang<sup>2</sup>, Wenjie Zhang<sup>6</sup>, Clara Grazian<sup>7,8</sup>, Chunyu Kit<sup>3</sup>,  
Wanli Ouyang<sup>5</sup>, Dongzhan Zhou<sup>5\*</sup>, Bram Hoex<sup>1\*</sup>

<sup>1\*</sup>School of Photovoltaic and Renewable Energy Engineering, University  
of New South Wales, Kensington, NSW, Australia.

<sup>2</sup>GreenDynamics, Sydney, NSW, Australia.

<sup>3</sup>Department of Linguistics and Translation, City University of Hong  
Kong, Hong Kong, China.

<sup>4</sup>Department of Computer Science, University of Wisconsin-Madison,  
Madison, Wisconsin, United States.

<sup>5</sup>Shanghai Artificial Intelligence Laboratory, Shanghai, China.

<sup>6</sup>School of Computer Science and Engineering, University of New South  
Wales, Kensington, NSW, Australia.

<sup>7</sup>School of Mathematics and Statistics, University of Sydney,  
Camperdown, NSW, Australia.

<sup>8</sup>DARE ARC Training Centre in Data Analytics for Resources and  
Environments, Camperdown, NSW, Australia.

\*Corresponding author(s). E-mail(s): [tong@greendynamics.com.au](mailto:tong@greendynamics.com.au);  
[zhoudongzhan@pjlab.org.cn](mailto:zhoudongzhan@pjlab.org.cn); [b.hoex@unsw.edu.au](mailto:b.hoex@unsw.edu.au);

<sup>†</sup>These authors contributed equally to this work.

## Abstract

Materials discovery and design aim to find compositions and structures with desirable properties over highly complex and diverse physical spaces. Traditional solutions, such as high-throughput simulations or machine learning, often rely on complex descriptors, which hinder generalizability and transferability across different material systems. Moreover, These descriptors may inadequately represent macro-scale material properties, which are influenced by structural imperfections and compositional variations in real-world samples, thus limiting their practical applicability. To address these challenges, we propose DARWIN 1.5, the largest

open-source large language model tailored for materials science. By leveraging natural language as input, DARWIN eliminates the need for task-specific descriptors and enables a flexible, unified approach to material property prediction and discovery. Our approach integrates 6M material domains papers and 21 experimental datasets from 49,256 materials across modalities while enabling cross-task knowledge transfer. The enhanced model achieves up to 59.1% improvement in prediction accuracy over the base LLaMA-7B architecture and outperforms SOTA machine learning approaches across 8 materials design tasks. These results establish LLMs as a promising foundation for developing versatile and scalable models in materials science.

**Keywords:** Large language models, AI for Science, material design, material science

## 1 Introduction

Materials innovation underpins technological progress across sectors, from clean energy and electronics to healthcare and transportation. The discovery and design of novel materials with enhanced properties can revolutionize existing technologies and enable entirely new applications, making it crucial for addressing global challenges like climate change [1, 2], sustainable development [3–5], and public health [6, 7]. However, materials discovery and design remains a complex endeavor, aiming to efficiently identify candidates with desired properties within a vast and complex space. This process faces challenges due to increasing structural and chemical diversity and complex structure-property-synthesis-performance relationships. The lack of a universal exploration method for the largely unlabeled materials data limits search efficiency. To address this, researchers employ two key approaches: (i) principle calculation, which provides accurate insights into material properties through high-throughput simulations [8–10], and (ii) machine learning (ML) techniques [11–13], which leverage growing materials datasets to expedite discovery workflows. Both strategies seek to navigate the complex materials landscape more efficiently, accelerating the discovery of new materials with targeted properties for various functional applications.

The adoption of ML in materials science faces significant challenges in developing universal input descriptors, primarily due to the disconnect between human-readable descriptions (e.g., “Tetragonal TiO<sub>2</sub>”) and machine-readable formats required for ML models (e.g., TiO<sub>2</sub> CIF file). This necessitates a complex translation process, often resulting in two key issues: (1) the creation of descriptors or features that lack generality, leading to poor transferability across different prediction tasks, and (2) overly complex model designs that further hinder broad applicability. Additionally, the heterogeneous nature of experimental materials, which often deviate from idealized material structures due to defects, impurities, or unique local environments, presents a significant obstacle. These real-world complexities are not easily captured by simplistic representations based on basic structural units, causing ML models to gauge the performance of experimental materials ineffectively. Consequently, there is a pressing need for a more sophisticated, flexible, and universal foundational model that can

effectively bridge the gap between human understanding, computational models, and experimental realities while remaining adaptable across diverse prediction tasks and material classes.

Large language models (LLMs), represented by ChatGPT [14], have captivated the academic community due to their proficiency in understanding directives and generating responses akin to human conversation. Compared to traditional ML methods taking carefully designed descriptors as inputs, such as random forest [15], SVM [16], and Gaussian Process [17], LLMs can directly process human-readable descriptions, which avoids the need for designing special input formats required for each task. Additionally, LLMs demonstrate potent generalization across various tasks, illustrating their capacity to resolve unseen or intricate challenges in natural science. [18, 19] are pioneering works in this direction, which demonstrate the efficacy of GPT models in solving chemical and material tasks, especially in the situation where available data are scarce, just as the wet-lab experimental scenarios. However, the core issue with these models lies in the fact that they remain inaccessible as open-source platforms, consequently compelling each user to engage in the laborious and financially burdensome task of individually fine-tuning the model on OpenAI’s servers. Furthermore, they fail to offer a robust degree of confidence in their precision, which reduces the trustworthiness and transparency of the model and thus can be viewed as a significant shortfall. Such constraints have the potential to impose a brake on the momentum at which LLMs are propelling scientific discovery.

In this work, we propose DARWIN 1.5, an open-source foundational LLM tailored for material science and chemistry. We design a two-stage training strategy, i.e., question-answering (QA) fine-tuning and multi-task learning to endow LLMs with the capability to proficiently perform these tasks. The QA dataset in the first stage is derived from highly-cited scientific literature, which not only facilitates the injection of critical ‘know-how’ knowledge into LLMs but also better emulates the paradigm by which human chemists or materials scientists perform tasks—by analyzing and interpreting literature, rather than exclusively relying on complex computational simulations such as operations involving CIF files.

Different from [18] that fine-tunes separate LLMs for each task, we employ a multi-task learning mechanism in the second stage to perform different tasks simultaneously, which consists of 5 classification and 17 regression tasks. These tasks are closely related to common material properties, which are mostly measured experimentally across diverse systems. This mechanism effectively leverages the synergy between tasks and mitigates the imbalance problem among data distribution, enabling shared learning of underlying representations and cross-task knowledge transfer. We conduct extensive experiments to validate the effectiveness of our approach, which achieves on-par or even better performance comparable with ML models across various tasks. Most importantly, our study highlights the potential of LLMs to internalize diverse types of data, paving the way toward the development of a universal model for chemistry and material science.

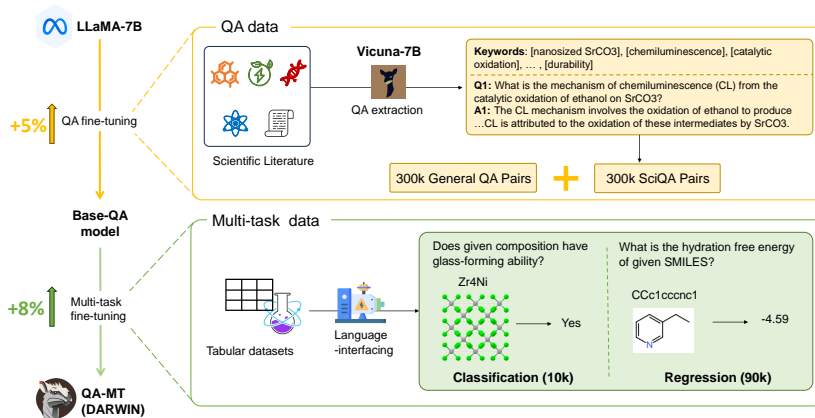


**Fig. 1** Overview of DARWIN. We adopt a two-stage training strategy, i.e., QA fine-tuning and multi-task learning, to achieve effective domain knowledge injection and enable the model to perform various core tasks in material and chemistry simultaneously.

## 2 Results

Recent works [18–21] have demonstrated the potential of LLM in materials science; however, these studies focused on fine-tuning separate models for individual property prediction tasks, leaving the potential of a unified predictive framework largely unexplored. Multi-task learning, as a ML strategy, offers a promising alternative by enabling models to simultaneously learn multiple related tasks through shared representations, thereby improving generalization capabilities [22]. It has demonstrated significant value in materials science by effectively capturing the inherent correlations among various material properties [23]. When applying this strategy in the materials domain, several key factors are usually considered: the careful identification and selection of physically meaningful features derived from descriptors associated with physical, chemical, and geometrical properties [24]; the reliance on standardized representation formats such as SMILES strings for polymeric materials [25] to ensure compatibility; and a focus on interrelated physical properties, such as Formation Energy ( $\Delta E^f$ ), Band Gap ( $E_g$ ), and Fermi Energy ( $E^F$ ) [23]. In contrast, LLMs have potential to bypass these constraints as inherently multi-task models. LLMs leverage natural language as a universal carrier of information, allowing them to process a diverse range of tasks and datasets without the need for domain-specific feature selection.

Building upon these foundations, we propose fine-tuning LLMs for multi-task materials property prediction. We examine 22 tasks transferred from 21 FAIR (Findable, Accessible, Interoperable, and Reusable) [26] datasets (‘Datasets’ section in Methods). These tasks comprise 5 classification problems and 17 regression problems, spanning diverse material systems from inorganics to composites. The datasets characterize fundamental physical, chemical, and electrochemical properties using various material

representations, including compositions, material names, and SMILES notations. The classification tasks predict discrete categories or labels, while the regression tasks focus on continuous numerical property values. When specific tasks are mentioned below, we include notes in parentheses after the task code about the input format and predicted property to aid understanding. To harness the full potential of LLMs for materials science applications, it is necessary to convert original datasets into a language-interfaced format suitable for fine-tuning these models. Inspired by Language-Interfaced Fine-Tuning (LIFT) [27], we design a set of prompt templates to convert samples in the 21 datasets into natural language sentences. The original data, which consists of material names (or representations) and outputs, such as labels or numeric values, is integrated with natural language descriptions of feature names and task-specific prompts. This leads to instructions that combine inputs and expected outputs. For example, an instruction may look like: ‘What is the band gap of given composition?’ with input ‘CdCu2SnS4’, and our model should give a text output ‘1.37’, which can be converted to a numeric value. To reduce hallucinations, we add 5% counterexamples in the training set of each task (‘Artificial counterexamples’ section in Method).

In addition to multi-task fine-tuning, we propose incorporating scientific QA fine-tuning to enhance the scientific reasoning capabilities of LLMs. This approach aims to mitigate the key limitation that existing ML applications often merely rely on specifically designed theoretical descriptors as inputs, which may not align well with experimental data and lead to potential discrepancies. To achieve this, we use SciQAG framework [28] to generate 332,997 open-ended scientific QA pairs (‘Datasets’ section in Methods) preserving essential information from lengthy scientific texts, which are particularly suitable for experimental contexts. We hypothesize that fine-tuning with such QA tasks enables the seamless integration of domain-specific “know-how” knowledge, thereby improving its adaptability across diverse tasks. To maintain the model’s general language capabilities and prevent overfitting to scientific content, we also include a comparable amount of general QA pairs from the Tulu dataset [29] in the training set. This balanced approach ensures the model retains robust general-purpose language understanding while gaining domain-specific scientific proficiency.

We explore the impact of QA and multi-task fine-tuning on 22 task performance using the open-source LLaMA-7B [30]. Our experimental setups include 4 specific fine-tuning strategies:

- 1) Single-task: we fine-tune the LLMs using a training set of each specific task, which allows us to assess the models’ ability to adapt to individual tasks and establish a baseline for a fair comparison. We obtain a fine-tuned model for each task in this setup, named ‘Base-ST’.

- 2) Multi-task: we fine-tune the LLMs using a mixture of all training datasets from 22 tasks. We obtained one fine-tuned model to perform all the tasks in this setup, named ‘Base-MT’.

- 3) QA-single (2-stage): we fine-tune the LLMs first on QA data (named ‘Base-QA’), then further fine-tune it using each specific task. In addition to the ‘Base-QA’ model, we obtain 22 fine-tuned models, denoted as ‘QA-ST’.

- 4) QA-multi (2-stage): we fine-tune the ‘Base-QA’ model using a mixture of all training datasets from 22 tasks, denoted as ‘QA-MT’.

## 2.1 Results of QA and multi-task fine-tuning

After fine-tuning the models, we evaluate their performance on the test data of each task separately (for each Base-ST and QA-ST model, we evaluate its performance on the corresponding test data). For classification tasks, we use the balanced macro F1-score, while for regression tasks, we employ mean absolute error (MAE). In Figure 2, we compare the task performance to figure out how different fine-tuning strategies influence the results. For classification tasks, QA fine-tuning leads to an average improvement of 1.55%, while multi-task fine-tuning results in an average improvement of 2.65%. The two-stage fine-tuning (QA-MT) achieves an average improvement of 3.38% compared to the Base-ST model. In regression tasks, QA fine-tuning yields an average improvement of 2.30%, while multi-task fine-tuning offers a significantly higher average improvement of 10.77%. Two-stage fine-tuning achieves the highest performance with a 11.79% improvement over the baseline. The results indicate that both QA fine-tuning and multi-task learning strategies contribute positively to the performance of LLMs. When used together, these strategies effectively inject the ‘know-how’ knowledge and leverage the synergistic effects between tasks, further enhancing the model’s capabilities.

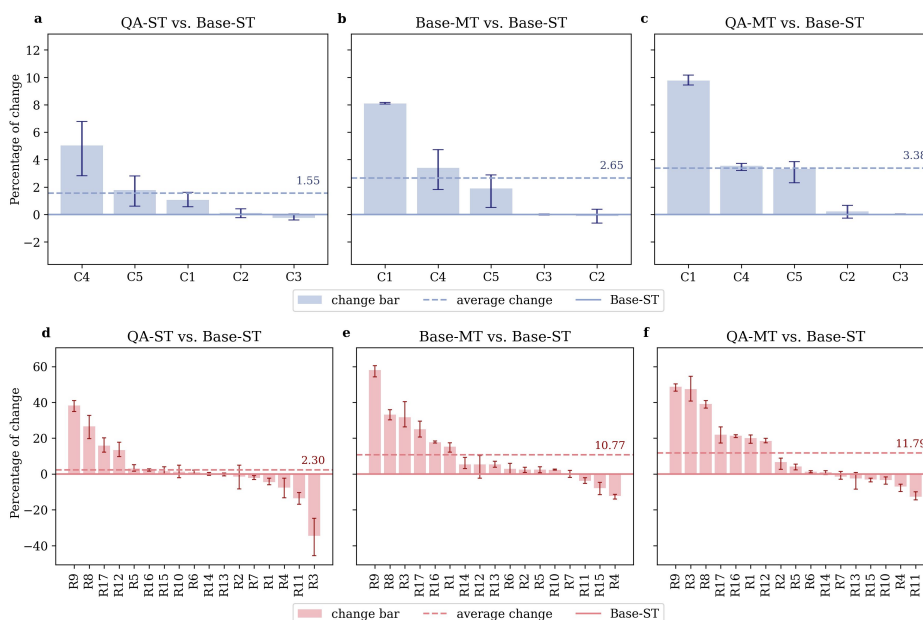


**Fig. 2** Comparison of different fine-tuning strategies on task performance. Base-ST is used as baseline and bars illustrate the difference between models on the specific tasks. The average improvement is indicated by the dashed line.

Different fine-tuning strategies demonstrate varying degrees of effectiveness across tasks. For example in Figure 2e, multi-task fine-tuning brings remarkable improvements to certain tasks, with R9 (SMILES, E isomer transition wavelength) showing

the highest enhancement of 58.12%. However, this same strategy leads to performance degradation in tasks like R4 (SMILES, lipophilicity), R5 (SMILES, log Henry’s Law constant for CO2), and R11 (composition, figure of merit) compared to the single-task baseline. This uneven distribution of improvements suggests that the effectiveness of each fine-tuning strategy is highly task-dependent. We hypothesize that this variation stems from inherent differences in inter-task relatedness during multi-task fine-tuning, which we systematically investigate through experiments detailed in [subsection 2.3](#).

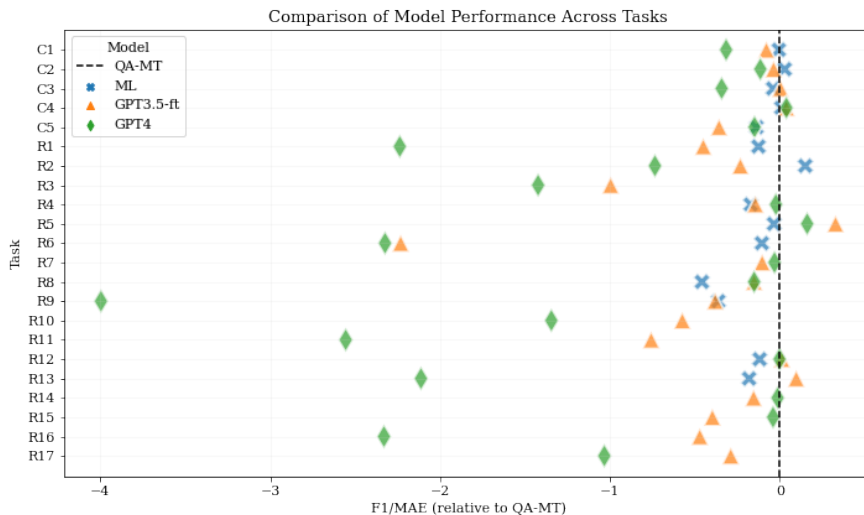


**Fig. 3** Comparison of model performance relative to QA-MT across tasks. Points on the left of the vertical line indicate poorer performance compared to QA-MT. The x-axis represents the performance ratio, where a value of -1 indicates performance 100% worse than QA-MT. For tasks with more than one ML results, the best one is used in this visualization.

When examining individual tasks’ responses to different fine-tuning strategies, we observe distinct patterns across classification and regression tasks. Among classification tasks, C1 (composition, metallicity), C4 (activated formula unit, water stability), and C5 (SMILES, absorption region) show consistent improvements across strategies, while C2 (composition, glass formation ability) and C3 (composition, alloy phase) demonstrate more modest gains. Notably, C1 achieves 1.06%, 8.09% and 9.76% improvement through three fine-tuning strategies respectively. The variation becomes even more pronounced in regression tasks. For example, R3 (composition, yield strength) performance shows a 34.57% decrease through QA fine-tuning (QA-ST), yet experiences significant improvements (31.77% and 47.51%) in both Base-MT and QA-MT. These contrasting outcomes suggest that while QA and multi-task fine-tuning may share some common beneficial elements, they ultimately contribute distinct forms of knowledge enhancement to the model. Two-stage fine-tuning demonstrates its advantage by effectively combining the strengths of both QA and multi-task approaches while relatively mitigating their respective limitations, as evidenced by its more balanced performance improvements across different tasks.

In [Figure 3](#), we compare the performance of QA-MT with closed-source GPT-series models and competitive ML algorithms (‘Machine learning results’ section in Methods). For the GPT-series, we conducted single-task fine-tuning experiments with GPT-3.5 and few-shot prompting with GPT-4 [\[31\]](#) (the maximum file upload size per fine-tuning job is limited to 16 MB and our data volume exceeded this size limitation for both the first-stage QA and the second-stage multi-task fine-tuning). The results show that QA-MT consistently outperforms GPT-3.5 (fine-tuned) and GPT-4 (few-shot) across most tasks. Notable exceptions are observed in tasks C4 (MOF, water stability) and R5 (SMILES, log Henry’s Law constant for CO<sub>2</sub>), where the GPT-series models slightly surpass QA-MT. Additionally, QA-MT achieves better performance than the ML baselines in 11 out of 14 tasks where ML baselines are available, highlighting its effectiveness in handling diverse material science applications.

We conducted further experiments to elucidate the mechanisms underlying the improved performance of LLM through 2-stage fine-tuning. In the following sections, we provide a detailed analysis of the key factors driving this enhancement.

## 2.2 Evaluating the impact of pre-training

We hypothesize that the general language capabilities acquired during the pre-training phase establish a robust foundation for subsequent QA fine-tuning and multi-task fine-tuning. To verify this, we conduct comparative experiments to assess the influence of pre-training in applying LLMs in material science. The fine-tuning strategies follow the same approaches as described earlier in (1) and (2), but with a key difference - we use an untrained LLaMA-7B model (with all parameters randomly initialized) as the base model. The single-task fine-tuning results in 22 specialized task models, referred to as “Random-ST” while the multi-task fine-tuning yields a single multi-task model, named “Random-MT”.

As shown in [Figure 4](#), when using the Random-ST as the comparison benchmark, we observe that the pre-trained model (Base-ST) achieves significantly better performance on single-task fine-tuning ([Figure 4a & 4d](#)): an average improvement of 11.04% on classification tasks and 33.57% on regression tasks. However, the gains from pre-training were not evenly distributed across tasks, varying from 83.3% (R9 in [Figure 4d](#)) to the negative (C4 in [Figure 4a](#)), which suggests that the background knowledge encoded during pre-training had varying degrees of relevance for different tasks. By comparing Random-MT and Random-ST ([Figure 4b & e](#)), we can observe the benefits of the multi-task fine-tuning strategy. Interestingly, the multi-task fine-tuning approach provided more remarkable improvements (8.08% on classification and 24.08% on regression) on the untrained model compared to the pre-trained counterpart (2.65% on classification and 10.77% on regression).

Comparing the gains from pre-training and multi-task fine-tuning ([Figure 4c & f](#)), we found that the latter could achieve near-equivalent performance to the former, albeit with slightly different emphases. This observation prompted further exploration of the distinct characteristics of these two approaches.

We hypothesize that the pre-training data contained a higher prevalence of more general material representations, such as material names and compositions, while more specialized expressions like SMILES and MOFs were less common. To investigate this,



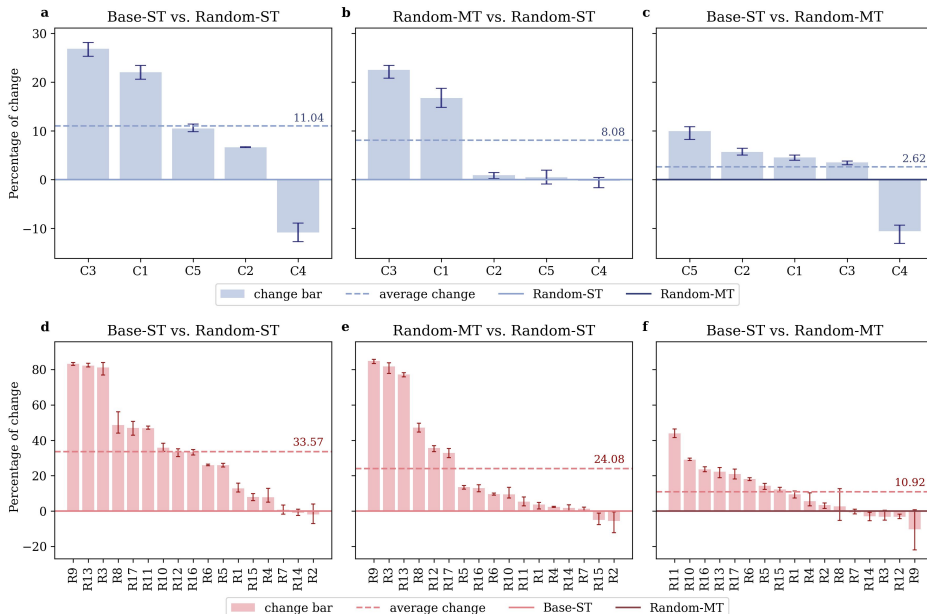


**Fig. 4** Comparative performance of pre-trained and non-pre-trained models under single-task and multi-task fine-tuning strategies. **a, d.** Single-task fine-tuning results, comparing pretrained (Base-ST) and non-pretrained (Random-ST) models. **b, e.** Multi-task fine-tuning results for non-pretrained (Random-MT) versus single-task non-pretrained (Random-ST) models. **c, f.** Comparison of pre-training and multi-task fine-tuning effects on overall performance. **a, b, c** show results on classification tasks and **d,e,f** show results on regression tasks.

we divided the 22 tasks into “general” (material names, compositions) and “specialized” (SMILES, MOFs) categories and compared the gains from pre-training and the different fine-tuning strategies. As shown in Figure 5, the pre-training-induced gains were more pronounced for the general category tasks, nearly double the specialized tasks. Similarly, the multi-task fine-tuning on the non-pretrained LLaMA model also benefited the general representation tasks more. However, when applied to the pre-trained LLaMA model, this categorical difference was less pronounced, suggesting that the general language capabilities acquired during pre-training underpin the domain-specific knowledge, and that language-interfaced multi-task fine-tuning can effectively leverage the knowledge encoded in LLMs to integrate diverse material representations, ultimately expanding their utility in natural sciences.

### 2.3 Investigating factors that affect prediction performance

Based on our observations from the preceding sections that multi-task fine-tuning demonstrated particularly significant improvements in regression tasks, we conducted detailed ablation studies using two widely recognized regression benchmark datasets from the materials science community: matbench\_exp\_bandgap and matbench\_steel.

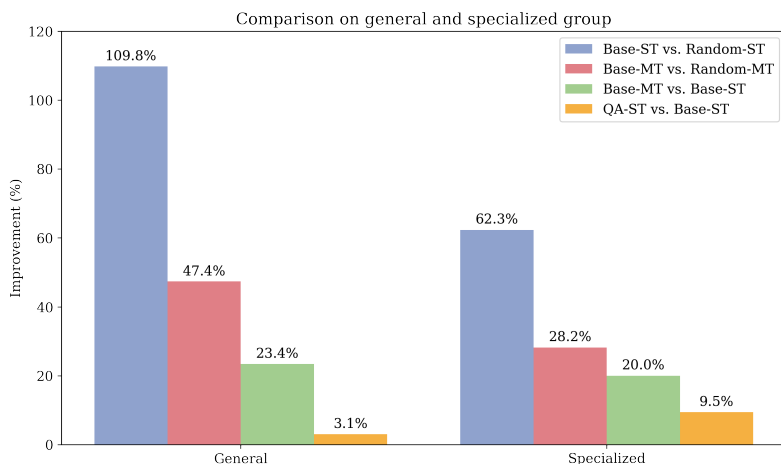


**Fig. 5** Comparative gains of pre-training and fine-tuning on general and specialized material representation tasks. This figure compares performance gains from pre-training and subsequent fine-tuning across two task categories: general (e.g., material names and compositions) and specialized (e.g., SMILES, MOFs).

To systematically investigate the mechanisms underlying the performance improvements, we designed multiple small-scale multi-task datasets by combining each target dataset with various auxiliary datasets:

Real dataset series:

- 1) +matbench: Incorporated three additional matbench tasks, all utilizing composition-based (general) material representations.
- 2) +other: Incorporated three tasks utilizing SMILES (specialized) representations, maintaining consistent total data volume.

Synthetic dataset series:

- 1) +Syn\_1: Generated from three matbench tasks, maintaining original composition inputs but replacing property values with random numbers within the original min-max range (right name, fabricated value).
- 2) +Syn\_2: Extended from +Syn\_1, replacing material compositions with randomly generated alphabetical codes (e.g., "ABC") (both fabricated).
- 3) +Syn\_3: Maintained original property values from the three matbench tasks but replaced material compositions with random alphabetical codes (fabricated name, right value).

We fine-tuned multiple models on LLaMA-7B using these auxiliary datasets and evaluated their performance on the original test sets. As illustrated in Figure 6, all auxiliary datasets except +Syn\_1 contributed to MAE reduction. Notably, the incorporation of incorrect property prediction data in +Syn\_1 led to performance deterioration, increasing the bandgap MAE from 0.386 to 0.659. This degradation suggests that +Syn\_1’s incorrect property data introduces misleading knowledge that compromises model performance. The performance improvement observed with +Syn\_2, despite its completely fabricated nature, demonstrates that model enhance its ability to correctly parse opened instructions and adhere to the specified requirements,

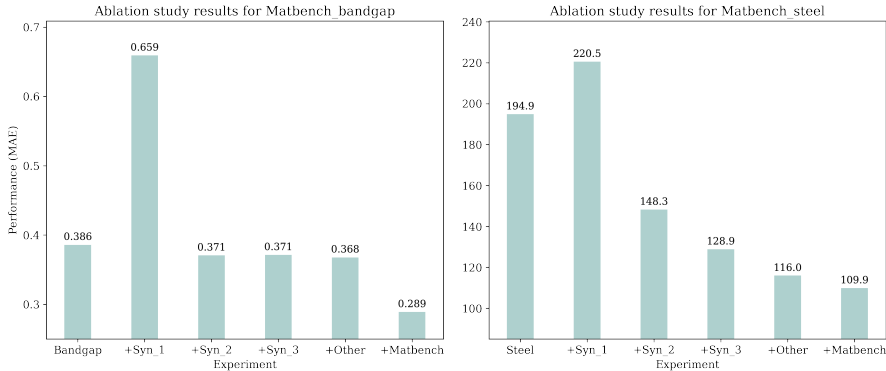


**Fig. 6** Ablation study to understand mechanisms behind multi-task fine-tuning improvements. To investigate why multi-task fine-tuning enhances performance, we conducted an ablation study using carefully constructed auxiliary datasets. The datasets were designed to isolate the effects of instruction format, real knowledge and material representation types.

which was defined as instruction-following ability [32], through pattern recognition in synthetic data structures. This finding suggests that the architectural benefits of multi-task learning persist even in the absence of meaningful domain knowledge. Exposure to a larger and more diverse set of training examples allows the model to better understand the nuances of the task and develop more robust and adaptable problem-solving strategies. The marginally superior performance of +Syn\_3 compared to +Syn\_2 indicates that maintaining authentic property distributions, even with fabricated material inputs, allows the model to capture underlying statistical patterns in materials property relationships.

The impact of authentic auxiliary data proved particularly illuminating. Both +other and +matbench datasets demonstrated substantially greater performance improvements compared to their synthetic counterparts, underscoring the importance of genuine materials science knowledge in model training. The superior performance of +matbench over +other provides compelling evidence for the advantage of general composition representations in knowledge transfer. In the case of matbench\_steel prediction, the reduction in MAE from 194.9 to 116.0 with +other, and to 109.9 with +matbench, representing an improvement of about 44% from the baseline performance. Comparing the performance improvements between +matbench and +Syn\_2 enables us to decompose the overall benefits of multi-task fine-tuning: while +Syn\_2 demonstrates the enhancement in instruction-following ability, the additional performance gains observed with +matbench can be attributed to the incorporation of domain-specific knowledge.

These observations corroborate our findings from the previous section: while LLMs can effectively learn and establish connections across specialized material representations through their general language capabilities and multi-task training, they demonstrate more comprehensive understanding and learning of materials expressed in general representations. These ablation experiments reveal that the success of multi-task fine-tuning extends beyond the model’s enhanced instruction-following

capabilities acquired from increased data exposure; it encompasses the understanding and acquisition of real-world knowledge. The pre-training phase of large language models serves as a fundamental bridge for connecting knowledge across different representational frameworks.

## 2.4 The application of QA-MT on bandgap prediction

The bandgap, a fundamental electronic property of materials, is the energy difference between the highest occupied molecular orbital (valence band) and the lowest unoccupied molecular orbital (conduction band). It plays a crucial role in determining a material’s electrical and optical properties, making it a key parameter in fields like transistors [33], photovoltaics [34], and light-emitting diodes (LEDs) [35]. For AI models in materials science, predicting bandgaps serves as a robust benchmark to evaluate their effectiveness and adaptability to domain-specific tasks. Accurate bandgap predictions can indicate a model’s capability in capturing essential material properties.

We compare several common methods for bandgap prediction with our QA-MT model, including:

1. Perdew–Burke–Ernzerhof (PBE) [36]: A generalized gradient approximation (GGA) functional for density functional theory (DFT) that improves upon local density approximation (LDA) by including electron density gradients.
2. Heyd–Scuseria–Ernzerhof (HSE) [37]: A hybrid functional that combines PBE with a fraction of exact exchange at short ranges, providing better accuracy but requiring more computational resources. Its accuracy for wide band gap materials can be enhanced by increasing the short-range Hartree-Fock exchange component, while maintaining semiconductor accuracy [38].
3. GW Approximation [39]: A many-body perturbation theory approach that calculates the electronic self-energy by expanding it in terms of the single particle Green’s function (G) and the screened Coulomb interaction (W).
4. AFLOW [40]: A PBE-trained ML model which predicts various material properties, including bandgaps, focusing on efficiency and scalability.

We predict bandgap for 7 specific compositions, unseen in QA-MT corresponding training set, that cover a wide energy range. These materials were chosen as test cases because researchers have thoroughly studied them using various theoretical methods, making them valuable benchmarks for evaluating new exchange-correlation functionals. Table 1 displays the results from each method, including Mean Absolute Deviation (MAD) and Root Mean Squared Error (RMSE) compared to experimental bandgap values ( $E_{g,exp}$ ). They both evaluate the error between predicted and observed values, while RMSE penalizes larger errors more significantly. As shown in the table, PBE method suffers from DFT systematic error and usually underestimates the bandgap values compared with the experimental  $E_{g,exp}$ . Compared with PBE, HSE raises more computational cost but the discrepancy between computation and experiment has undoubtedly been reduced. GW, the most complex and computationally expensive one, shows the most accurate results (0.12 MAD and 0.15 RMSE) for test cases. Compared with these first-principle methods, AFLOW has improved based on PBE but still far from HSE, with lower inference costs and faster speed as a ML algorithm. It also has same systematic error as PBE since it trained using PBE values. Our model

QA-MT achieves a MAD of 0.51 and an RMSE of 0.65, which are comparable to the HSE results. This shows that our model, while not reaching GW’s accuracy, performs significantly better than other methods like PBE and AFLOWE.

**Table 1** Comparison of simulation methods for bandgap prediction with QA-MT (DARWIN).

Compos.	$E_{g,exp}$	$E_{g,PBE}$	$E_{g,HSE}$	$E_{g,GW}$	$E_{g,AFLOW}$	$E_{g,QA-MT}$
GaN	3.2 [41]	1.62 [41] (-49%)	3.14 [42] (-2%)	3.32 [41] (4%)	1.85 (-42%)	2 (-38%)
CdTe	1.6 [43]	0.62 [44] (-61%)	1.52 [44] (-3%)	1.76 [43] (12%)	0.67 (-57%)	1.08 (-33%)
ZnS	3.91 [41]	2.07 [41] (-47%)	3.49 [42] (-11%)	4.15 [41] (6%)	2.6 (-33%)	2.9 (-26%)
Cu <sub>2</sub> ZnSnS <sub>4</sub>	1.6 [45]	0.28 [45] (-83%)	0.09 [45] (-94%)	1.64 [45] (3%)	N/A	1.46 (-8.8%)
PbTe	0.19 [41]	0 [41] (-100%)	0.19 [46] (0%)	0.26 [41] (36%)	0 (-100%)	0.3 (58%)
GaAs	1.52 [41]	0.19 [41] (-86%)	1.12 [42] (-26%)	1.52 [41] (0%)	0.24 (-84%)	1.18 (-22%)
ZnO	3.44 [41]	0.67 [41] (-81%)	2.49 [42] (-28%)	3.2 [41] (-7%)	1.87 (-46%)	3.2 (-7.0%)
MAD		1.43	0.49	0.12	1.11	0.51
RMSE		1.61	0.71	0.15	1.19	0.65

Note: The units of bandgap in the table are all electronvolts (eV). Mean Absolute Deviation (MAD) and Root Mean Squared Error (RMSE) are calculated with respect to the experimental values. Percentage under each calculated value is also shown compared to the corresponding experimental value. The bandgap values in AFLOW column are reported from [40].

In conclusion, QA-MT demonstrates strong predictive capability for bandgaps, showcasing the potential of advanced language models in materials science. It offers three key advantages over current methods. The first advantage is its accuracy. The training of QA-MT incorporates experimental data, making its predictions much closer to experimentally measured band gaps, and it avoids the system errors associated with methods like PBE and AFLOW. A second significant advantage of QA-MT is its minimal input requirements. Unlike DFT-based simulations, which require detailed structural information such as atomic positions and lattice parameters, QA-MT only needs the material composition as input. In this study, we utilized the composition of each material (e.g., “GaN” or “CdTe”) to make predictions, without relying on additional structural details. This low barrier to input data enables QA-MT to be applied in scenarios where structural data may be incomplete, costly, or unavailable. Lastly, QA-MT stands out for its rapid inference speed. While traditional simulation methods

are computationally intensive and can take hours or even days for complex materials, QA-MT can predict band gaps almost instantaneously. This speed makes it highly suitable for high-throughput screening, allowing researchers to explore large chemical spaces more efficiently. Overall, the combination of speed, minimal input requirements, and competitive accuracy makes QA-MT a powerful tool for materials property prediction, underscoring the growing role of language models as an efficient and versatile alternative to traditional simulation-based approaches in materials science.

### 3 Conclusion

In this study, we probed both the capabilities and underlying mechanisms of large language models in materials science through systematic investigation. Our multi-stage training approach demonstrates that LLMs can effectively internalize materials science knowledge across multiple systems and modalities - from structural information and synthesis protocols to characterization techniques and performance metrics. By leveraging natural language as the interface, we establish a fundamentally different paradigm from traditional computational approaches. While our model accepts compositional information as input, our investigations reveal it develops sophisticated understanding of the materials space through exposure to scientific literature and multi-task training data, learning the complex relationships between composition, structure, synthesis, and properties.

Our systematic investigation revealed three key findings. First, the QA-multi (2-stage) strategy succeeds by combining scientific literature understanding with multi-task prediction capabilities. This approach outperformed traditional methods and even showed competitive results with GPT-3.5 fine-tuning and GPT-4 prompting across diverse materials prediction tasks. Second, our ablation studies demonstrated that exposure to diverse task formats enhances the model’s instruction-following capabilities, while training across multiple tasks enables better statistical learning of property distributions and facilitates knowledge transfer between related properties. Third, the model develops a sophisticated understanding of materials relationships that goes beyond simple pattern matching, as evidenced by its performance on carefully designed synthetic datasets maintaining authentic property distributions.

The broader implications of this work extend beyond technical metrics, demonstrating a fundamental shift in how we can approach materials science. Unlike traditional first-principles methods that scale up from atomic or molecular levels, our approach leverages humanity’s accumulated scientific knowledge, captured in natural language, to create quantitative experiential models that can guide materials design. This achievement essentially creates a "materials science GPT" - a foundational model that learns and reasons about materials in ways that parallel human scientific thinking. The model’s ability to process natural language descriptions and integrate knowledge across multiple domains opens new possibilities for materials discovery and design.

Looking ahead, our mechanistic understanding opens several promising research directions. Future work should focus on exploring targeted pre-training strategies that enhance specific capabilities identified in our ablation studies, developing new multi-task learning or multi modality architectures, like CLIP [47], LLaVA [48], that

better leverage the synergies we discovered among different materials, and investigating how LLMs understand and represent the materials space. By illuminating the mechanisms behind their performance, we enable more informed development of future foundational models for scientific discovery. The synergistic combination of pre-trained capabilities, multi-task learning, and domain-specific knowledge, understood through our systematic investigations, promises to accelerate the discovery and development of new materials for critical applications across science and technology.

## 4 Methods

### 4.1 Datasets

To improve the capability of LLMs, we generated scientific QA pairs as training set of QA fine-tuning using SciQAG framework [28]. The main idea is to train a QA generator to convert full-text scientific papers into QA pairs and use an evaluator to filter out those that do not meet quality standards. The task of QA generator is defined as follows: given seed input texts  $T$ , for each input text  $t$ , the generator should firstly generate 15 keywords  $k$  that capture the most important terms and concepts in the text, then generate a set  $S = \{(q_i, a_i)\}_{i=1}^n$  focusing on the generated keywords  $k$ , where  $\forall i \in \{1, \dots, 10\}$ ,  $q_i$  is the question and  $a_i$  is the answer to  $q_i$ . To generate  $S$ , one should learn a generator  $G(S|T; \theta)$  with  $\theta$  the model parameters. Thus, given a new input text  $\hat{t}$ , following  $G(S|T; \theta)$ , one can directly generate a  $\hat{S}$  consisting of QA pairs (by firstly generating 15 keywords to guide the QA generation). To fine-tune an open-source LLM as QA generator, we first randomly selected 700 papers from the paper collection as input to produce 7000 seed QA pairs by prompting GPT-4 (see Appendix D). Then, we fine-tuned llama3-64k model [49] on seed data. The data employs the instruction schema [50] composed of three elements: <instruction>, <input>, and <output>. The seed QA generation prompt was converted into the <instruction>. The seed paper filled the <input> field, and the <output> were the generated seed QA pairs. We concatenated the instruction and instance input as a prompt and train the model to generate the instance output in a standard supervised way. Using the trained QA generator, we performed inference on the remaining papers to form a training set. To reduce the occurrence of article-specific information in questions (i.e., non-knowledge-based questions that can only be answered using the given article information), a simple rule-based approach was used to remove all pairs containing “this paper” or “this study”. The distribution of scientific QA categories of final 332,997 QA pairs can be found in B.

FAIR stands for 'Findable, Accessible, Interoperable, and Reusable', which is a set of principles for enhancing the value and accessibility of data [26]. Due to the strong impact of 4V (volume, variety, velocity, and veracity) of big data on materials science, efforts have been made in recent years to collect comprehensive data from research groups worldwide, including unpublished data, and ensure its FAIRness [51]. We collect 21 open-accessed FAIR datasets from highly cited publications in materials science. 5 classification tasks and 17 regression tasks are derived from these datasets according to their property types. It is important to note that there is not a one-to-one correspondence between tasks and datasets. In some cases, multiple tasks are

derived from a single dataset. For instance, from the MoosaviDiversity dataset [52], we construct two regression tasks, R5 and R6, which predict the log Henry’s Law constant for CH4 and CO2, respectively, based on SMILES representations. Conversely, some datasets are consolidated into a single task to prevent data leakage. For example, both the ESOL [53] and DLS-100 [54] datasets, which focus on solubility prediction, are merged into a single regression task (R17). The details of these datasets and visualization can be found in A and B. Following task partitioning, we design prompt templates to transform tabular data samples into natural language sentences suitable for each task. These templates follow an instruction-based format to align with the LLaMA fine-tuning paradigm. Detailed specifications of the prompt templates and exemplar instructions for each task are provided in C.

## 4.2 Artificial counterexamples

One prevalent issue with LLMs is the generation of hallucinations—incorrect or fabricated information presented as factual [55]. To address this, we explored the effectiveness of incorporating artificial counterexamples into the fine-tuning process of LLMs. Our hypothesis is that by exposing the model to deliberately incorrect information during training, the model learns to distinguish between factual data and potential hallucinations. This pilot study was designed to address several research questions: 1) Does the inclusion of counterexamples in the fine-tuning process reduce the occurrence of hallucinations? 2) Does the integration of counterexamples during training negatively impact the model’s performance on the normal test set? 3) Is there a correlation between the proportion of counterexamples included in training and the reduction of hallucinations?

To answer above questions, we selected 2 classification tasks, 3 regression tasks that require the model to generate or infer detailed scientific information, such as predicting whether a composition is glass. Due to adherence to the format during fine-tuning, the model tends to predict whether nearly all inputs using format trained. For example, it predicts “farmer” as FALSE (not glass), even though “farmer” is not even a composition. This is clearly inconsistent with the facts. For each task selected, we created artificial counterexamples which involve intentionally providing incorrect or irrelevant inputs that don’t match the expected types (see Data in Methods section). We then fine-tuned the model with varying ratios of these counterexamples integrated into the 500 training samples, specifically 0% (baseline), 1%, 2%, 5%, 10% and 20% of the total training data. The evaluation had two stages: First, we assessed the model’s performance on a 100-sample test set without fabrications, recording metrics like MAE and F1-score to see if counterexamples affected its primary function. Second, we tested with 100 artificial counterexamples to evaluate the model’s accuracy in identifying and handling hallucinations, focusing on rejecting false information and maintaining output integrity.

As shown in Figure 7, the results indicate that incorporating counterexamples into the training procedure effectively reduces hallucinations. Models trained with counterexamples exhibited a marked decrease in the generation of incorrect information during the counterexample test evaluation. For instance, with a 5% ratio of counterexamples, hallucinations were reduced by approximately 100% compared to the



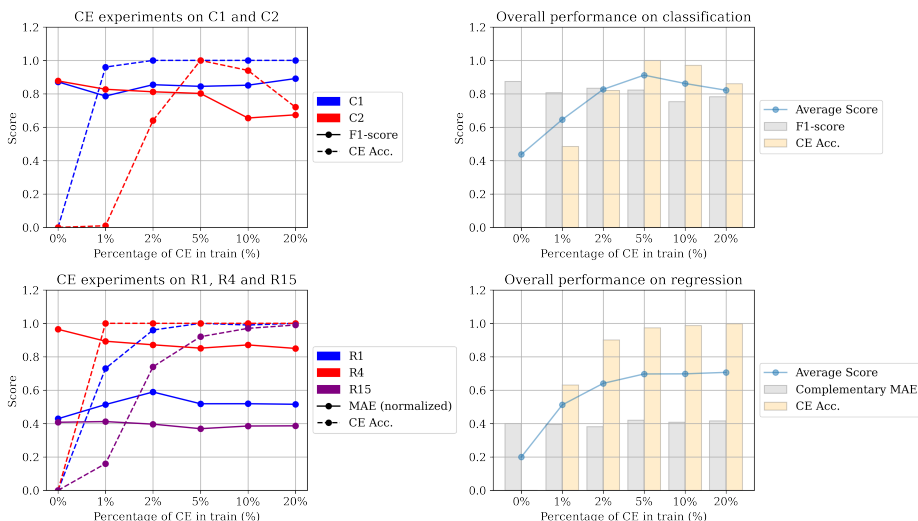


**Fig. 7** Results of counterexample experiments.

baseline. Importantly, the inclusion of counterexamples did not significantly impair the model’s performance on normal test evaluations, with metrics such as MAE and F1-score remaining stable across small counterexample ratios. This suggests that the model can learn to identify and reject false information without compromising its ability to process and generate accurate data for standard tasks. Thus, for most ML training data in this study, we generate 5% counterexamples and mix them with the original dataset. By fine-tuning models with a carefully balanced dataset that includes both normal and “noisy” examples, we can enhance the reliability of these models in producing factual and trustworthy outputs.

### 4.3 Machine learning baselines

We include results from several ML models as references, like CrabNet [56], MODNet (v0.1.1) [57], and AMMExpress v2020 from matbench [58] and ML algorithm Gaussian process regression (GPR) used in GPTchem [18]. For some tasks, we directly use the ML result from its original papers of FAIR dataset. It should be noted that ML result of each task was individually trained on a specific single-task data. Take GPR for R1 and GPR for R2 as an example, they are results from two GPR models trained on R1 and R2 task data, respectively. For each ML algorithm we used in this study, it usually receives only one kind of input format and does not have results for all tasks. And due to different representation formats of the input, not all tasks have ML baselines. For example, R16 task data contains common names of the materials which cannot be converted into input of ML algorithms. The detail results of these datasets and which tasks they are used to derive instructions can be found in Appendix Table F.

## 4.4 Fine-tuning strategy

For all QA-generator model, QA-base model and ST/MT models, We fine-tune the LLaMA models following established methods, using a setup of 4×AMD MI250X GPUs and employing the Brain Floating Point 16 (BF16) data format for an optimal balance between precision and computational efficiency. For the LLaMA-3-8B-16k model, which is for QA generation, we adopt the LongLoRA [59] method with Flash-Attention2 [60] and DeepSpeed stage 3 [61]. Training is conducted for 5 epochs with a per-device batch size of 1, maximum sequence length of 16,000, and gradient accumulation over 8 steps. The learning rate is set to 2e-5 with no weight decay, and warm-up steps are set to 20. For inference, we use a temperature of 0.6 and top\_p of 0.9 for logical and diverse text generation.

Similarly, for QA-base model and MT model, the LLaMA-7b model is fine-tuned based on Stanford’s Alpaca approach. DeepSpeed stage 2 [61] is employed with a batch size of 2 per device, maximum sequence length of 512, and gradient accumulation over 4 steps. The learning rate remains 2e-5 with no weight decay, while a warm-up ratio of 0.03 is applied. These configurations are tailored to handle the shorter QA and task sequences efficiently.

Due to the large volume of QA samples, we train for 3 epochs to avoid overfitting, with training completion in approximately 15 hours. For fine-tuning on single- and multi-task datasets, we increase the training to 5 epochs, with multi-task fine-tuning taking about 4 hours to complete. During inference, we set the temperature to 0.8 and top\_p to 0.75, which makes text generated more logical with rich vocabulary.

In experiments involving the `gpt-series` models, we use `gpt-3.5-turbo-0613` for fine-tuning and `gpt-4-0613` for few-shot learning. For training, we utilize default parameters determined algorithmically by Azure OpenAI based on the size of the training data. During inference, we set the temperature to 0.8 to enhance generation diversity.

## Declarations

### Funding

This research was supported by generous funding and resources from multiple organizations. We gratefully acknowledge the support of: 1) The Australian Supercomputing Facility, which provided critical computational resources essential to our research infrastructure. 2) Microsoft Corporation, whose technological support and computational resources were instrumental in advancing our project. 3) The Australian Renewable Energy Agency (ARENA), whose financial support and commitment to innovative energy research made this work possible. 4) The Australian Centre for Advanced Photovoltaics (ACAP), whose funding and scientific collaboration significantly contributed to our research outcomes.

We extend our sincere thanks to these organizations for their crucial support in enabling this research endeavor.

## Competing interests

The authors declare no competing interests.

## Ethics approval and consent to participate

Not applicable

## Consent for publication

Not applicable

## Materials availability

Not applicable

## Data availability

The multi-task fine-tuning datasets used in this study, including training sets, test sets, small-scale multi-task datasets (subsection 2.3) are available via Figshare at 10.6084/m9.figshare.28023626. The weights of QA-MT model are provided in the Onedrive link in <https://github.com/MasterAI-EAM/Darwin>.

## Code availability

The source code is freely available at <https://github.com/MasterAI-EAM/Darwin> under an MIT license. The versions of the packages used in the study are provided in the requirements file in GitHub repository.

## Appendix A Details of datasets

**Table A1:** Details of FAIR datasets and associated tasks they are used to derive instructions, (R for regression; C for classification)

Dataset	Description	Task Code
Matbench_is_metal [58]	This dataset is retrieved from Zhuo et al.’s work, containing data on classifying metallicity from composition for 4921 chemical formulas.	C1
Matbench_glass [62]	This dataset is retrieved from a volume of the Landolt–Börnstein collection ‘Nonequilibrium phase diagrams of ternary amorphous alloys’, containing data on full bulk metallic glass formation ability for 5680 chemical formulas.	C2

Pei [63]	The dataset consists of 1252 observations with 625 single-phase and 627 multi-phase alloys, covering binaries and multi-component systems. We constructed a binary classification task on phase of alloys.	C3
WaterStability [64]	The dataset consists of water stabilities for over 200 MOFs (metal-organic frameworks), alongside a comprehensive set of chemical features encompassing the metal node, organic ligand, and metal-ligand molar ratios. We constructed 170 pairs of activated formula unit and its stability (high or low) from training set. The activated formula unit is the "cleaned up" version of the structure after removing any solvent molecules or unbound guests, showing just the essential framework components and their ratios.	C4
UV [65]	This dataset includes 18,309 records of experimentally determined UV/vis absorption maxima, and associated extinction coefficients. We constructed a subset of 5,158 SMILES with absorption region classification (ultraviolet or visible).	C5
NagasawaOPV [66]	1203 experimental parameters of organic photovoltaic (OPV) materials are manually collected from the literature and subjected to machine learning with digitized chemical structures. We constructed 3 regression tasks by using SMILES to predict bandgap, highest occupied molecular orbital (HOMO) and polydispersity index (PDI)	R1, R2
Matbench_steels [58]	This dataset is retrieved from Citrine informatics, containing data on steel yield strengths from composition for 312 chemical formulas	R3
ChEMBL [67]	This dataset is sourced from a curated database of bioactive molecules with drug-like properties, focusing on the lipophilicity of 1899 molecular compounds in pharmacokinetics. The water-octanol partition coefficient (logD) is used to describe lipophilicity.	R4

MoosaviDiversity [52]	A diverse set of structures based on the chemical and geometric descriptors CH <sub>4</sub> , CO <sub>2</sub> . We constructed 5941 samples of SMILES and log Henry’s Law constant for CH <sub>4</sub> and CO <sub>2</sub> using experimental part, which is actually from CoRE-2019 [68].	R5, R6
MoosaviCp [69]	Dataset for predicting the heat capacity of materials based on density functional theory simulations	R7
FreeSolv [70]	This dataset provides experimental and calculated hydration free energies for small molecules in water, along with experimental values and input files. We constructed 641 samples of SMILES and its hydration free energy.	R8
photoswitch [71]	The dataset includes experimentally-determined properties for 405 photoswitches. We constructed a regression task to predict E isomer transition wavelength of given SMILES.	R9
SuperCon_ML [72]	This work considers over 16,000 different compositions from SuperCon [73] database for machine learning. It houses information such as the critical temperature (T <sub>c</sub> ) and reporting journal publication for superconducting materials known from experiment. We extracted a list of 10,436 compounds with T <sub>c</sub> reported.	R10
UCSB+ESTM [74, 75]	UCSB is a database of about 1,100 experimental thermoelectric materials from UCSB aggregated from 108 source publications and personal communications. ESTM is a public database of thermoelectric materials and system-identified material representation for data-driven discovery. We made a combination and cleaning of UCSB and ESTM to predict thermoelectric figure of merit (zT) of 5747 composition with temperature conditions.	R11

TADF [76]	A database of thermally activated delayed fluorescent (TADF) molecules was automatically generated from the scientific literature. Among these, 5,349 records have chemical names in the form of SMILES strings which are represented with 91% accuracy. We constructed delayed lifetime (435 samples), emission wavelength (937 samples), and photoluminescence quantum yield (719 samples) of SMILES.	R12, R13, R14
Refractive [77]	The database comprises a total of 49,076 refractive index and 60,804 dielectric constant data records on 11,054 unique chemicals. We constructed 6,262 pairs of compound and its refractive index.	R15
Matbench_expt_gap [78]	This dataset is retrieved from Zhuo et al.’s work, containing data on experimental band gaps and DFT calculated zero band gaps for 4604 compounds.	R16
Semiconductor [79]	This work presents an auto-generated database of 100,236 semiconductor band gap records, extracted from 128,776 journal articles with their associated temperature information. We constructed 5,000 samples of material name and its averaged bandgap.	R16
QMUG [80]	The QMUG collection comprises quantum mechanical properties of more than 665 k biologically and pharmacologically relevant molecules. We constructed 6592 samples of SMILES and its HOMO-LUMO gap.	R16
ESOL [53]	This dataset is a compilation of measured aqueous solubility (LogS) values, a crucial factor in drug discovery. The dataset comprises 927 molecular compounds originally used for ESOL - estimated solubility.	R17
DLS-100 [54]	A set of 100 molecules with measured and reported intrinsic aqueous solubilities, together with a suggested 75-25 training-test split.	R17

## Appendix B Dataset visualization

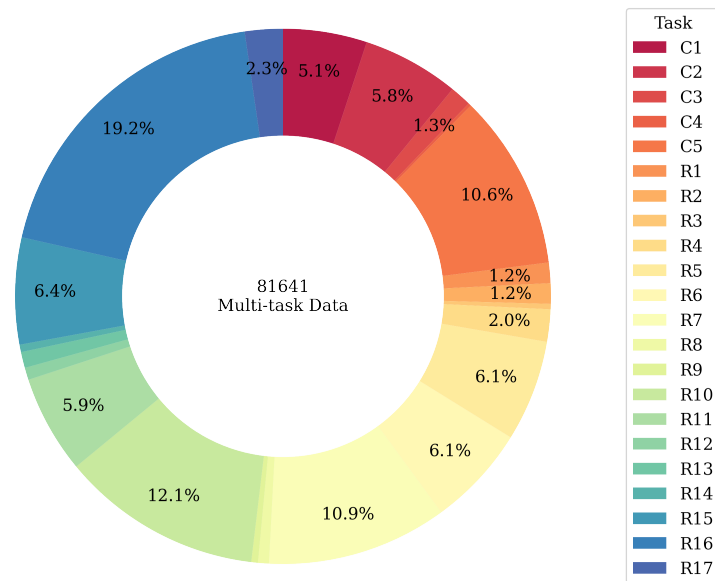


**Fig. B1** Visualization of multi-task dataset size. Labels of all percentages below 1% are hidden.

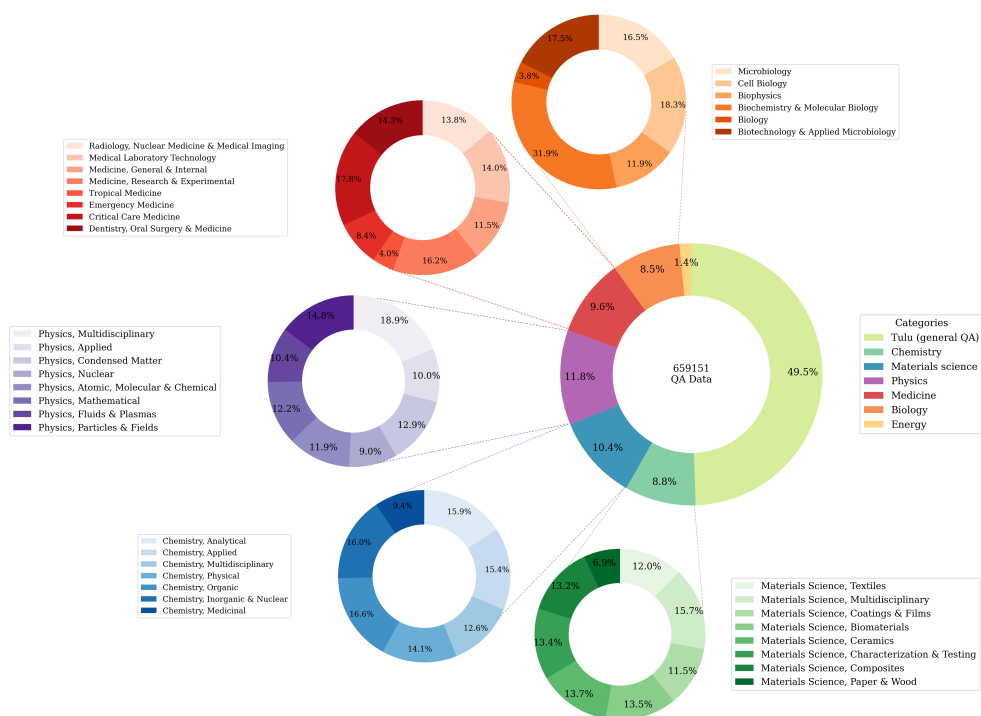


Fig. B2 Visualization of QA data categories.

## Appendix C Templates for converting tabular data to sentences

### Label definition

**<material\_type>**: The specific format (e.g. composition) used to represent a material's characteristics or structure.

**<material\_representation>**: The actual representation of material (e.g. TiO<sub>2</sub>), typically showing its elemental composition or structural details.

**<yes\_no>**: A binary response indicating the presence or absence of a specific characteristic. The format typically follows the pattern "Yes/No".

**<has\_>**: A linguistic marker that indicates the presence or absence of a specific material property or characteristic, typically used to explicitly state whether a material possesses a particular attribute. It connects the material representation with a specific property in a grammatically complete statement. The format typically follows the pattern "has/have/does not have".

**<property>**: A characteristic or attribute (e.g. bandgap) of a material that describes its behavior, performance, or physical characteristics.

**<property\_value>**: The numerical or quantitative measurement of a specific property of the material.



- **Classification templates**

**Template 1:**

**Instruction:** Tell me if given <material\_type> <has.> <property>.

**Input:** <material\_representation>

**Output:** <yes\_no>, <material\_representation> <has.> <property>.

**Template 2:**

**Instruction:** Does given <material\_type> <has.> <property>?

**Input:** <material\_representation>

**Output:** <yes\_no>, <material\_representation> <has.> <property>.

- **Regression templates**

**Template 1:**

**Instruction:** Given a <material\_type>, write its <property>.

**Input:** <material\_representation>

**Output:** <property\_value>.

**Template 2:**

**Instruction:** Predict the <property> of this given <material\_type>.

**Input:** <material\_representation>

**Output:** <property\_value>.

**Template 3:**

**Instruction:** What is the <property> of this given <material\_type>?

**Input:** <material\_representation>

**Output:** <property\_value>.

Note: The above templates are applicable to data conversion for most tasks, with individual tasks having some adjustments. Please refer to the following examples for specifics.

- **Classification tasks**

**C1 data example:**

**Instruction:** Tell me if this composition is a metal.

**Input:** BaAg2

**Output:** Yes, BaAg2 is a metal.

**C2 data example:****Instruction:** Tell me if given composition has glass formation ability.**Input:** Cr23Ni17Mo10**Output:** Yes, Cr23Ni17Mo10 has glass formation ability.**C3 data example:****Instruction:** Predict the phase of this given alloy.**Input:** Al1Co1Cr1Cu1Fe1Mo0.4Ni1**Output:** multi-phase**C4 data example:****Instruction:** Predict the water stability of this given activated formula unit.**Input:** Cr(OH)1,4-benzenedicarboxylate**Output:** high**C5 data example:****Instruction:** Given this SMILES, predict whether the compound would absorb light in the ultraviolet region or the visible region?**Input:** Cr(OH)1,4-benzenedicarboxylate**Output:** high

- **Regression tasks**

**R1 data example:****Instruction:** Predict the highest occupied molecular orbital (HOMO) of this given SMILES.**Input:** CC1=CC2=C(C(SC(C3=CC=C(C)C4=NSN=C43)=C5)=C5N2C(CCCCC)C(CCC)S1**Output:** 4.81**R2 data example:****Instruction:** What is the poly dispersity index (PDI) of this given SMILES?**Input:** CC(S1)=CC2=C1C(OCCCCCCCCCCC)=C(C=C(C3=C4C(OCCO4)=C(C)S3)S5)C5=C2OCCCCCCCCCCC**Output:** 1.9**R3 data example:****Instruction:** Given a composition, write its yield strength.**Input:** Fe0.768Co0.000931Mn0.00244Si0.00199Cr0.110Ni0.0981Mo0.0113V0.000110Nb0.0000602Co0.0000948Al0.00497Ti0.00269**Output:** 1167.2

**R4 data example:****Instruction:** What is the lipophilicity of given SMILES?**Input:** CC(C)OC(=O)N1CCC(CC1)Oc2ncnc(Oc3ccc(cc3F)S(=O)(=O)C)c2C**Output:** 3.54**R5 data example:****Instruction:** Predict the the log Henry's Law constant for CO2 of given SMILES.**Input:** [Co].c1ccc(cn1)[CH][N][N][CH]c1cccnc1**Output:** -1.726468633**R6 data example:****Instruction:** What is the the log Henry's Law constant for CH4 of given SMILES?**Input:** N#Cc1cccc(c1)CN1CCN(CC1)Cc1cccc(c1)C#N.[Ag]**Output:** -4.259713121**R7 data example:****Instruction:** What is the gravimetric heat capacity at 300 K of this MOF with given features and topology?**Input:** linker [O-]C(=O)c1cc([O])c(cc1[O])C(=O)[O-], nodes [Ni], topology pcu**Output:** 15.84091337**R8 data example:****Instruction:** Given this SMILES, write its hydration free energy.**Input:** c1ccc(cc1)c2ccccc2**Output:** -2.7**R9 data example:****Instruction:** Predict the E isomer transition wavelength of given SMILES.**Input:** CC(N(C)C(C)=C1C)=C1/N=N/C2=CC=CC=C2**Output:** 345.0**R10 data example:****Instruction:** Predict the critical temperature Tc in Kelvin K for a given superconductor composition.**Input:** Ni2.5Cu1.5Zr8**Output:** 1.09**R11 data example:****Instruction:** Given composition with temperature conditions, write its thermoelectric

figure of merit (zT).

**Input:** composition: Ti0.99Nb0.01NiSn, temperature (K):400.0

**Output:** 0.203822375

**R12 data example:**

**Instruction:** What is the photoluminescence quantum yield (%) of given SMILES?

**Input:** O=C1c2ccccc2C(=O)c2cc(Sc3ccc(-n4c5ccccc5c5ccccc54)cc3)ccc21

**Output:** 1.8

**R13 data example:**

**Instruction:** Given this SMILES, write its maximum emission wavelength (nm).

**Input:** c1ccc2c(c1)nc1n(-c3ccc(-c4ccc5oc6ccccc6c5c4)cn3)c3ccccc3n21

**Output:** 483.0

**R14 data example:**

**Instruction:** What is the delayed lifetime ( $\mu\text{s}$ ) of given SMILES?

**Input:** O=C(c1ccc(N2c3ccccc3Oc3ccccc32)cc1)c1cccc(C(=O)c2ccc(N3c4ccccc4Oc4ccc43)cc2)n1

**Output:** 1.0

**R15 data example:**

**Instruction:** Given this compound, write its averaged refractive index.

**Input:** CsNO3

**Output:** 1.3479

**R16 data example:**

**Instruction:** What is the averaged band gap of given material?

**Input:** heptazine

**Output:** 2.7

**R17 data example:**

**Instruction:** Given a SMILES, write its water solubility expressed as a logarithm in mol/L.

**Input:** c1cc2ccc3cccc4c3c2c(c1)cc4

**Output:** -6.18

## Appendix D Prompt for scientific QA generator

Here is a scientific paper:

{text}

Given the provided scientific paper, please complete the following two steps:

Step 1: Keyword Extraction

Read the scientific paper and identify 15 keywords that capture the most important terms and concepts in the paper, avoiding generic or broad terms. Compile the selected keywords into a list.

Step 2: Question-Answer Generation

Generate 10 scientific question-answer pairs as diverse as possible based on facts and knowledge presented in the given paper, focusing on keywords you generated. Keep the following requirements in mind: Avoid asking simple or definitional questions. Assume that the reader does not have access to the original paper or any external sources, so ensure that the questions and answers are self-contained and do not rely on references to figures, tables, or other parts of the paper. Incorporate specific data and insights from the paper to provide detailed and informative answers. Keep the answers concise, accurate, and directly related to the corresponding questions.

Please present the generated keywords and question-answer pairs in the following format:

Keywords: [keyword 1], [keyword 2], ..., [keyword15]

Q1: [Question 1]

A1: [Answer 1]

Q2: [Question 2]

A2: [Answer 2]

...

Q10: [Question 10]

A10: [Answer 10]

## Appendix E Scientific QA examples

Q1: What is Type 1 diabetes and what causes it?

A1: Type 1 diabetes is an autoimmune disease that results from the selective destruction of insulin-producing beta cells in the pancreatic islets. Genetics, environmental factors, nutritional effects, and a combination of these are believed to be associated with the disease. Streptozotocin (STZ) is commonly used to induce diabetes mellitus in experimental studies.

Q2: What is the role of metabolomics in healthcare?

A2: Metabolomics is a rapidly growing field that relates biological end points to multiple altered metabolite concentrations, providing a wealth of biological information on complex systems. It has been applied to a variety of diseases such as cancer, type 2 diabetes, and inborn errors of metabolism. It uses advanced analytical techniques such as nuclear magnetic resonance (NMR) spectroscopy and mass spectrometry with multivariate statistical analysis to identify potential biomarkers and biological networks.

Q3: How was the diabetic rat model established in this study?

A3: In this study, female rats were divided into a diabetic group and a control group. The diabetic group received an intraperitoneal dose of STZ, and showed glucose levels in the blood of more than 200 mg/dl after 4 days. The control group was matched for age and gender, and did not receive the STZ injection.

Q4: What were the key findings regarding glucose metabolism in the study?

A4: The study found that in diabetes, glucose excretion was enormous, being nearly 7500-fold higher than in control rats. Other significantly enhanced metabolites included lactate, alanine, ethanol, and fumarate. These findings suggest that glucose metabolism is dramatically perturbed in diabetes.

Q5: What is the importance of the Cori cycle in maintaining glucose homeostasis?

A5: The Cori cycle, also known as the glucose-lactate cycle, is a metabolic pathway that plays a crucial role in maintaining glucose homeostasis. It involves the conversion of glucose, lactate, and alanine, and is responsible for producing Cori cycle intermediates, which are used in gluconeogenesis precursor production and facilitating glucose oxidation.

Q6: What is the role of acetate switch in metabolism?

A6: The acetate switch, also known as the molecular switch that regulates the dissimilation and assimilation of acetate, plays a role in accumulating an acetyl-coenzyme A (CoA) pool due to both exogenous (bacterial fermentation) and endogenous (mammalian) production. This accumulation can have significant implications for metabolism.

Q7: How did the urinary metabolites differ between diabetic and control rats in the study?

A7: The urinary metabolites showed dramatic changes in the rat diabetic model when compared with blood-based assays. Glucose was the most notable metabolite in diabetic urine, with very high-intensity signals. Other metabolites such as alanine, lactate, ethanol, acetate, and fumarate also showed significant increases in the diabetic group.

Q8: What was the effect of STZ administration on plasma glucose levels?

A8: Following STZ administration, plasma glucose showed elevated levels, with its quantity being nearly three times higher than in control rats.

Q9: What were some of the changes observed in the rat diabetic model's blood parameters?

A9: Other than the significant increases in blood glucose levels, the study also observed elevated levels of urea and creatinine, and decreased levels of plasma protein and cholesterol in diabetic rats.

Q10: How did the correlations among the detected metabolites differ between the diabetic and control rats?

A10: The correlations among the detected metabolites showed a number of striking differences between the diabetic and control rats. For example, the correlation of glucose with alanine was increased in diabetic rats, while the correlation of glucose with lactate decreased. These changes indicate significant alterations in metabolism in the diabetic rats.

## Appendix F Machine learning results

**Table F2:** Results of machine learning baselines

Task	GPR	CrabNet	Matbench	Original paper
C1		0.961	0.92 (AMMExpress)	
C2		0.909	0.97 (MODNet)	
C3				0.93 [63]
C4				0.86 [64]
C5	0.7037			
R1	0.11			
R2	0.857			
R3		182.94		
R4	1.024			
R5	0.5622			0.51 [52]
R6	0.2412			0.2 [52]
R7				
R8	0.623			
R9	10.286			
R10				
R11				
R12	23.713			
R13	46.332			
R14	129.667			
R15				
R16				
R17				

## Appendix G LoRA Results

**Table G3:** Results of LoRA Fine-Tuning on Each FAIR Task

Task	LlaMA-ST	QA-ST
C1	0.4682	0.6567
C2	0.726	0.8365

<b>Task</b>	<b>LlaMA-ST</b>	<b>QA-ST</b>
C3	0.3333	0.4
C4	0.4	0.898
C5	0.1932	0.6672
R1	0.3466	7.2155
R2	1.3111	1.414
R3	1566.5858	1187.3564
R4	1.4021	3.0897
R5	3.7006	5.4472
R6	1.34	8.7431
R7	6.0984	255.4198
R8	5.0269	62.7915
R9	328.4036	316.985
R10	15.4674	22.5444
R11	0.3712	17.4563
R12	34.5563	48.3285
R13	105.1862	189.57778
R14	429.3761	147.708
R15	1.3875	2.1887
R16	0.7663	7.1009
R17	2.6799	8.9210



## Appendix H Bandgap prediction visualization

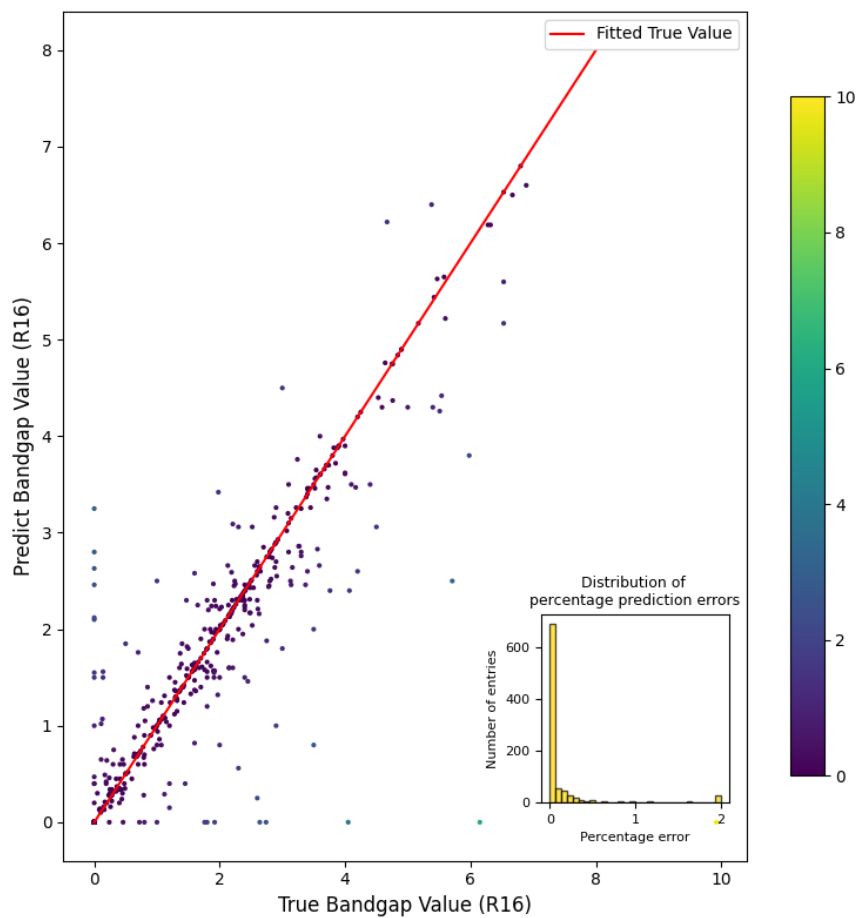


**Fig. H3** Comparison between true and predicted bandgap values, with percentage error

## References

- [1] Zhong, M., Tran, K., Min, Y., Wang, C., Wang, Z., Dinh, C.-T., De Luna, P., Yu, Z., Rasouli, A.S., Brodersen, P., *et al.*: Accelerated discovery of co2 electrocatalysts using active machine learning. *Nature* **581**(7807), 178–183 (2020)
- [2] Shi, X.-L., Zou, J., Chen, Z.-G.: Advanced thermoelectric design: from materials and structures to devices. *Chemical reviews* **120**(15), 7399–7515 (2020)
- [3] Zhang, S., Liu, Z., Zhang, W., Jiang, Z., Chen, W., Chen, R., Huang, Y., Yang, Z.,

- Zhang, Y., Han, L., *et al.*: Barrier designs in perovskite solar cells for long-term stability. *Advanced Energy Materials* **10**(35), 2001610 (2020)
- [4] Acik, M., Darling, S.B.: Graphene in perovskite solar cells: device design, characterization and implementation. *Journal of Materials Chemistry A* **4**(17), 6185–6235 (2016)
- [5] Song, R., Murphy, M., Li, C., Ting, K., Soo, C., Zheng, Z.: Current development of biodegradable polymeric materials for biomedical applications. *Drug design, development and therapy*, 3117–3145 (2018)
- [6] Li, W., Thian, E.S., Wang, M., Wang, Z., Ren, L.: Surface design for antibacterial materials: from fundamentals to advanced strategies. *Advanced Science* **8**(19), 2100368 (2021)
- [7] Law, K.L., Narayan, R.: Reducing environmental plastic pollution by designing polymer materials for managed end-of-life. *Nature Reviews Materials* **7**(2), 104–116 (2022)
- [8] Xi, L., Pan, S., Li, X., Xu, Y., Ni, J., Sun, X., Yang, J., Luo, J., Xi, J., Zhu, W., *et al.*: Discovery of high-performance thermoelectric chalcogenides through reliable high-throughput material screening. *Journal of the American Chemical Society* **140**(34), 10785–10793 (2018)
- [9] Curtarolo, S., Setyawan, W., Hart, G.L., Jahnatek, M., Chepulskii, R.V., Taylor, R.H., Wang, S., Xue, J., Yang, K., Levy, O., *et al.*: Aflow: An automatic framework for high-throughput materials discovery. *Computational Materials Science* **58**, 218–226 (2012)
- [10] Brunin, G., Ricci, F., Ha, V.-A., Rignanese, G.-M., Hautier, G.: Transparent conducting materials discovery using high-throughput computing. *npj Computational Materials* **5**(1), 63 (2019)
- [11] Deringer, V.L., Caro, M.A., Csányi, G.: Machine learning interatomic potentials as emerging tools for materials science. *Advanced Materials* **31**(46), 1902765 (2019)
- [12] Cui, T., Tang, C., Su, M., Zhang, S., Li, Y., Bai, L., Dong, Y., Gong, X., Ouyang, W.: Gpip: Geometry-enhanced pre-training on interatomic potentials. arXiv preprint arXiv:2309.15718 (2023)
- [13] Zhang, D., Liu, X., Zhang, X., Zhang, C., Cai, C., Bi, H., Du, Y., Qin, X., Peng, A., Huang, J., *et al.*: Dpa-2: a large atomic model as a multi-task learner. *npj Computational Materials* **10**(1), 293 (2024)
- [14] OpenAI: GPT-4 Technical Report. Preprint at <https://arxiv.org/abs/2303.08774> (2023)

- [15] Breiman, L.: Random forests. *Machine learning* **45**, 5–32 (2001)
- [16] Cortes, C.: Support-vector networks. *Machine Learning* (1995)
- [17] Rasmussen, C.E.: Gaussian processes in machine learning. In: *Summer School on Machine Learning*, pp. 63–71. Springer, ??? (2003)
- [18] Jablonka, K.M., Schwaller, P., Ortega-Guerrero, A., Smit, B.: Leveraging large language models for predictive chemistry. *Nature Machine Intelligence* **6**(2), 161–169 (2024)
- [19] Xie, T., Wan, Y., Zhou, Y., Huang, W., Liu, Y., Linghu, Q., Wang, S., Kit, C., Grazian, C., Zhang, W., et al.: Creation of a structured solar cell material dataset and performance prediction using large language models. *Patterns* **5**(5) (2024)
- [20] Jacobs, R., Polak, M.P., Schultz, L.E., Mahdavi, H., Honavar, V., Morgan, D.: Regression with large language models for materials and molecular property prediction. Preprint at <https://arxiv.org/abs/2409.06080> (2024)
- [21] Rubungo, A.N., Arnold, C., Rand, B.P., Dieng, A.B.: Llm-prop: Predicting physical and electronic properties of crystalline solids from their text descriptions. Preprint at <https://arxiv.org/abs/2310.14029> (2023)
- [22] Ruder, S.: An Overview of Multi-Task Learning in Deep Neural Networks. Preprint at <https://arxiv.org/abs/1706.05098> (2017)
- [23] Sanyal, S., Balachandran, J., Yadati, N., Kumar, A., Rajagopalan, P., Sanyal, S., Talukdar, P.: Mt-cgcnn: Integrating crystal graph convolutional neural network with multitask learning for material property prediction. Preprint at <https://arxiv.org/abs/1811.05660> (2018)
- [24] De Breuck, P.-P., Hautier, G., Rignanese, G.-M.: Materials property prediction for limited datasets enabled by feature selection and joint learning with modnet. *npj computational materials* **7**(1), 83 (2021)
- [25] Kuenneth, C., Rajan, A.C., Tran, H., Chen, L., Kim, C., Ramprasad, R.: Polymer informatics with multi-task learning. *Patterns* **2**(4) (2021)
- [26] Wilkinson, M.D., Dumontier, M., Aalbersberg, I.J., Appleton, G., Axton, M., Baak, A., Blomberg, N., Boiten, J.-W., da Silva Santos, L.B., Bourne, P.E., Bouwman, J., Brookes, A.J., Clark, T., Crosas, M., Dillo, I., Dumon, O., Edmunds, S., Evelo, C.T., Finkers, R., Gonzalez-Beltran, A., Gray, A.J.G., Groth, P., Goble, C., Grethe, J.S., Heringa, J., 't Hoen, P.A.C., Hooft, R., Kuhn, T., Kok, R., Kok, J., Lusher, S.J., Martone, M.E., Mons, A., Packer, A.L., Persson, B., Rocca-Serra, P., Roos, M., Schaik, R., Sansone, S.-A., Schultes, E., Sengstag, T., Slater, T., Strawn, G., Swertz, M.A., Thompson, M., Lei, J., Mulligen, E., Velterop, J., Waagmeester, A., Wittenburg, P., Wolstencroft, K., Zhao, J., Mons, B.: The FAIR

Guiding Principles for scientific data management and stewardship. *Scientific Data* **3**(1), 160018 (2016) <https://doi.org/10.1038/sdata.2016.18>

- [27] Dinh, T., Zeng, Y., Zhang, R., Lin, Z., Gira, M., Rajput, S., Sohn, J.-y., Papailiopoulos, D., Lee, K.: Lift: Language-interfaced fine-tuning for non-language machine learning tasks. *Advances in Neural Information Processing Systems* **35**, 11763–11784 (2022)
- [28] Wan, Y., Ajith, A., Liu, Y., Lu, K., Grazian, C., Hoex, B., Zhang, W., Kit, C., Xie, T., Foster, I.: SciQAG: A Framework for Auto-Generated Scientific Question Answering Dataset with Fine-grained Evaluation. Preprint at <https://arxiv.org/abs/2405.09939> (2024)
- [29] Ivison, H., Wang, Y., Pyatkin, V., Lambert, N., Peters, M., Dasigi, P., Jang, J., Wadden, D., Smith, N.A., Beltagy, I., Hajishirzi, H.: Camels in a Changing Climate: Enhancing LM Adaptation with Tulu 2. Preprint at <https://arxiv.org/abs/2311.10702> (2023)
- [30] Touvron, H., Lavril, T., Izacard, G., Martinet, X., Lachaux, M.-A., Lacroix, T., Rozière, B., Goyal, N., Hambro, E., Azhar, F., et al.: Llama: Open and efficient foundation language models. arXiv preprint arXiv:2302.13971 (2023)
- [31] Achiam, J., Adler, S., Agarwal, S., Ahmad, L., Akkaya, I., Aleman, F.L., Almeida, D., Altenschmidt, J., Altman, S., Anadkat, S., et al.: Gpt-4 technical report. arXiv preprint arXiv:2303.08774 (2023)
- [32] Zeng, Z., Yu, J., Gao, T., Meng, Y., Goyal, T., Chen, D.: Evaluating large language models at evaluating instruction following. Preprint at <https://arxiv.org/abs/2310.07641> (2023)
- [33] Radisavljevic, B., Radenovic, A., Brivio, J., Giacometti, V., Kis, A.: Single-layer mos2 transistors. *Nature nanotechnology* **6**(3), 147–150 (2011)
- [34] Polman, A., Knight, M., Garnett, E.C., Ehrler, B., Sinke, W.C.: Photovoltaic materials: Present efficiencies and future challenges. *Science* **352**(6283), 4424 (2016)
- [35] Schubert, E.F., Kim, J.K.: Solid-state light sources getting smart. *Science* **308**(5726), 1274–1278 (2005)
- [36] Perdew, J.P., Burke, K., Ernzerhof, M.: Generalized gradient approximation made simple. *Physical review letters* **77**(18), 3865 (1996)
- [37] Heyd, J., Scuseria, G.E.: Efficient hybrid density functional calculations in solids: Assessment of the heyd–scuseria–ernzerhof screened coulomb hybrid functional. *The Journal of chemical physics* **121**(3), 1187–1192 (2004)

- [38] Garza, A.J., Scuseria, G.E.: Predicting band gaps with hybrid density functionals. *The journal of physical chemistry letters* **7**(20), 4165–4170 (2016)
- [39] Gerosa, M., Bottani, C.E., Caramella, L., Onida, G., Di Valentin, C., Pacchioni, G.: Electronic structure and phase stability of oxide semiconductors: Performance of dielectric-dependent hybrid functional dft, benchmarked against gw band structure calculations and experiments. *Physical Review B* **91**(15), 155201 (2015)
- [40] Isayev, O., Oses, C., Toher, C., Gossett, E., Curtarolo, S., Tropsha, A.: Universal fragment descriptors for predicting properties of inorganic crystals. *Nature communications* **8**(1), 15679 (2017)
- [41] Shishkin, M., Kresse, G.: Self-consistent gw calculations for semiconductors and insulators. *Physical Review B—Condensed Matter and Materials Physics* **75**(23), 235102 (2007)
- [42] Tran, F., Blaha, P.: Accurate band gaps of semiconductors and insulators;? format?¿ with a semilocal exchange-correlation potential. *Physical review letters* **102**(22), 226401 (2009)
- [43] Zakharov, O., Rubio, A., Blase, X., Cohen, M.L., Louie, S.G.: Quasiparticle band structures of six ii-vi compounds: Zns, znse, znTe, cds, cdse, and cdte. *Physical Review B* **50**(15), 10780 (1994)
- [44] Heyd, J., Peralta, J.E., Scuseria, G.E., Martin, R.L.: Energy band gaps and lattice parameters evaluated with the heyd-scuseria-ernzerhof screened hybrid functional. *The Journal of chemical physics* **123**(17) (2005)
- [45] Zhao, H., Persson, C.: Optical properties of cu (in, ga) se<sub>2</sub> and cu<sub>2</sub>znSn (s, se) 4. *Thin Solid Films* **519**(21), 7508–7512 (2011)
- [46] Skelton, J.M., Parker, S.C., Togo, A., Tanaka, I., Walsh, A.: Thermal physics of the lead chalcogenides pbs, pbse, and pbte from first principles. *Physical Review B* **89**(20), 205203 (2014)
- [47] Radford, A., Kim, J.W., Hallacy, C., Ramesh, A., Goh, G., Agarwal, S., Sastry, G., Askell, A., Mishkin, P., Clark, J., *et al.*: Learning transferable visual models from natural language supervision. In: *International Conference on Machine Learning*, pp. 8748–8763 (2021). PMLR
- [48] Liu, H., Li, C., Wu, Q., Lee, Y.J.: Visual instruction tuning. *Advances in neural information processing systems* **36** (2024)
- [49] AI@Meta: Llama 3 Model Card. GitHub[https://github.com/meta-lama/llama3/blob/main/MODEL\\_CARD.md](https://github.com/meta-lama/llama3/blob/main/MODEL_CARD.md) (2024)

- [50] Wang, Y., Kordi, Y., Mishra, S., Liu, A., Smith, N.A., Khashabi, D., Hajishirzi, H.: Self-instruct: Aligning language model with self generated instructions. Preprint at <https://arxiv.org/abs/2212.10560> (2022)
- [51] Scheffler, M., Aeschlimann, M., Albrecht, M., Bereau, T., Bungartz, H.-J., Felser, C., Greiner, M., Groß, A., Koch, C.T., Kremer, K., *et al.*: Fair data enabling new horizons for materials research. *Nature* **604**(7907), 635–642 (2022)
- [52] Moosavi, S.M., Nandy, A., Jablonka, K.M., Ongari, D., Janet, J.P., Boyd, P.G., Lee, Y., Smit, B., Kulik, H.J.: Understanding the diversity of the metal-organic framework ecosystem. *Nature communications* **11**(1), 1–10 (2020)
- [53] Delaney, J.S.: Esol: estimating aqueous solubility directly from molecular structure. *Journal of chemical information and computer sciences* **44**(3), 1000–1005 (2004)
- [54] McDonagh, J.L., Nath, N., De Ferrari, L., Van Mourik, T., Mitchell, J.B.: Uniting cheminformatics and chemical theory to predict the intrinsic aqueous solubility of crystalline druglike molecules. *Journal of chemical information and modeling* **54**(3), 844–856 (2014)
- [55] Xu, Z., Jain, S., Kankanhalli, M.: Hallucination is inevitable: An innate limitation of large language models. Preprint at <https://arxiv.org/abs/2401.11817> (2024)
- [56] Wang, A.Y.-T., Kauwe, S.K., Murdock, R.J., Sparks, T.D.: Compositionally restricted attention-based network for materials property predictions. *Npj Computational Materials* **7**(1), 77 (2021)
- [57] Breuck, P.-P.D., Evans, M.L., Rignanese, G.-M.: Robust model benchmarking and bias-imbalance in data-driven materials science: a case study on MODNet. *Journal of Physics: Condensed Matter* **33**(40), 404002 (2021) <https://doi.org/10.1088/1361-648x/ac1280>
- [58] Dunn, A., Wang, Q., Ganose, A., Dopp, D., Jain, A.: Benchmarking materials property prediction methods: the matbench test set and automatminer reference algorithm. *npj Computational Materials* **6**(1), 138 (2020)
- [59] Chen, Y., Qian, S., Tang, H., Lai, X., Liu, Z., Han, S., Jia, J.: LongLoRA: Efficient Fine-tuning of Long-Context Large Language Models (2023)
- [60] Dao, T.: FlashAttention-2: Faster Attention with Better Parallelism and Work Partitioning (2023)
- [61] Rasley, J., Rajbhandari, S., Ruwase, O., He, Y.: DeepSpeed: System optimizations enable training deep learning models with over 100 billion parameters. In: *Proceedings of the 26th ACM SIGKDD International Conference on Knowledge Discovery & Data Mining*, pp. 3505–3506 (2020). <https://doi.org/10.1145/>

- [62] Kawazoe, Y., Yu, J.-Z., Tsai, A.-P., Masumoto, T.: Nonequilibrium phase diagrams of ternary amorphous alloys. Springer (1997)
- [63] Pei, Z., Yin, J., Hawk, J.A., Alman, D.E., Gao, M.C.: Machine-learning informed prediction of high-entropy solid solution formation: Beyond the hume-rothery rules. *npj Computational Materials* **6**(1), 50 (2020)
- [64] Batra, R., Chen, C., Evans, T.G., Walton, K.S., Ramprasad, R.: Prediction of water stability of metal–organic frameworks using machine learning. *Nature Machine Intelligence* **2**(11), 704–710 (2020)
- [65] Beard, E.J., Sivaraman, G., Vázquez-Mayagoitia, Á., Vishwanath, V., Cole, J.M.: Comparative dataset of experimental and computational attributes of uv/vis absorption spectra. *Scientific data* **6**(1), 307 (2019)
- [66] Nagasawa, S., Al-Naamani, E., Saeki, A.: Computer-aided screening of conjugated polymers for organic solar cell: classification by random forest. *The Journal of Physical Chemistry Letters* **9**(10), 2639–2646 (2018)
- [67] Gaulton, A., Bellis, L.J., Bento, A.P., Chambers, J., Davies, M., Hersey, A., Light, Y., McGlinchey, S., Michalovich, D., Al-Lazikani, B.: ChEMBL: a large-scale bioactivity database for drug discovery. *Nucleic acids research* **40**(D1), 1100–1107 (2012)
- [68] Chung, Y., Haldoupis, E., Bucior, B., Haranczyk, M., Lee, S., Vogiatzis, K., Ling, S., Milisavljevic, M., Zhang, H., Camp, J., et al.: Computation-Ready Experimental Metal-Organic Framework (CoRE MOF) 2019 Dataset. Zenodo <https://doi.org/10.5281/zenodo> (2019)
- [69] Moosavi, S.M., Novotny, B.Á., Ongari, D., Moubarak, E., Asgari, M., Kadioglu, Ö., Charalambous, C., Ortega-Guerrero, A., Farmahini, A.H., Sarkisov, L., et al.: A data-science approach to predict the heat capacity of nanoporous materials. *Nature materials* **21**(12), 1419–1425 (2022)
- [70] Mobley, D.L., Guthrie, J.P.: Freesolv: a database of experimental and calculated hydration free energies, with input files. *Journal of computer-aided molecular design* **28**, 711–720 (2014)
- [71] Griffiths, R.-R., Greenfield, J.L., Thawani, A.R., Jamasb, A.R., Moss, H.B., Bourached, A., Jones, P., McCorkindale, W., Aldrick, A.A., Fuchter, M.J., et al.: Data-driven discovery of molecular photoswitches with multioutput gaussian processes. *Chemical Science* **13**(45), 13541–13551 (2022)
- [72] Stanev, V., Oses, C., Kusne, A.G., Rodriguez, E., Paglione, J., Curtarolo, S., Takeuchi, I.: Machine learning modeling of superconducting critical temperature.

- npj Computational Materials **4**(1), 29 (2018)
- [73] Materials Science, M.I.S.: SuperCon. [http://supercon.nims.go.jp/index\\_en.html](http://supercon.nims.go.jp/index_en.html) (2011)
- [74] Gaultois, M.W., Sparks, T.D., Borg, C.K., Seshadri, R., Bonificio, W.D., Clarke, D.R.: Data-driven review of thermoelectric materials: performance and resource considerations. *Chemistry of Materials* **25**(15), 2911–2920 (2013)
- [75] Na, G.S., Chang, H.: A public database of thermoelectric materials and system-identified material representation for data-driven discovery. *npj Computational Materials* **8**(1), 214 (2022)
- [76] Huang, D., Cole, J.M.: A database of thermally activated delayed fluorescent molecules auto-generated from scientific literature with chemdataextractor. *Scientific Data* **11**(1), 80 (2024)
- [77] Zhao, J., Cole, J.M.: A database of refractive indices and dielectric constants auto-generated using chemdataextractor. *Scientific data* **9**(1), 192 (2022)
- [78] Zhuo, Y., Mansouri Tehrani, A., Brgoch, J.: Predicting the band gaps of inorganic solids by machine learning. *The journal of physical chemistry letters* **9**(7), 1668–1673 (2018)
- [79] Dong, Q., Cole, J.M.: Auto-generated database of semiconductor band gaps using chemdataextractor. *Scientific Data* **9**(1), 193 (2022)
- [80] Isert, C., Atz, K., Jiménez-Luna, J., Schneider, G.: Qmugs, quantum mechanical properties of drug-like molecules. *Scientific Data* **9**(1), 273 (2022)